

# Landau level degeneracy and quantum Hall effect in a graphite bilayer

Edward McCann and Vladimir I. Fal'ko

*Department of Physics, Lancaster University, Lancaster, LA1 4YB, United Kingdom*

We derive an effective two-dimensional Hamiltonian to describe the low energy electronic excitations of a graphite bilayer in a magnetic field. At high magnetic field, its Landau level spectrum consists of almost equidistant groups of fourfold degenerate states at finite energy and eight states at zero energy. This can be translated into the Hall conductivity dependence on carrier density,  $\sigma_{xy}(N)$ , which exhibits plateaus at integer values of  $4e^2/h$  and has a “double”  $8e^2/h$  step between the hole and electron gases across zero density, in contrast to half-integer sequencing in a monolayer.

PACS numbers: 73.63.Bd, 71.70.Di, 73.43.Cd, 81.05.Uw

Electronic transport properties of a graphite monolayer have for many decades attracted theoretical interest due to a Dirac-like spectrum of charge carriers [1, 2, 3, 4, 5, 6] in this gapless semiconductor [7]. Until recently, this material remained illusive experimentally and the thinnest graphitic films studied contained dozens of atomic layers, exhibiting essentially properties of bulk graphite. However, last year Novoselov *et al.* [8] fabricated ultra-thin graphitic devices only a few-layers thick including monolayer structures. This was rapidly followed by several further reports [9, 10, 11] in which Shubnikov de Haas oscillations and the Hall effect were studied in structures containing a small number of layers. It has turned out to be a particular challenge in these experiments to distinguish between single and two-layer systems [10, 12]. In this Letter we show that degeneracies in the Landau level spectrum of a graphite bilayer determine a sequencing of plateaus in the quantum Hall effect conductivity  $\sigma_{xy}(N)$  which may be used to differentiate it from a monolayer material. This statement is based upon the analysis of the effective low energy Hamiltonian describing the two-dimensional electron (hole) gas in a bilayer with a low carrier density  $N \lesssim 10^{13} \text{cm}^{-2}$ .

We model a graphite bilayer as two coupled hexagonal lattices including inequivalent sites  $A, B$  and  $\tilde{A}, \tilde{B}$  in the bottom and top layers, respectively, which are arranged according to Bernal ( $\tilde{A}$ - $B$ ) stacking [7, 13, 14], as shown in Fig. 1. A lattice with such symmetry supports a degeneracy point at each of two inequivalent corners,  $K$  and  $\tilde{K}$ , of the hexagonal Brillouin zone [15], which coincide with the Fermi point in a neutral structure and determine the centers of two valleys of a gapless spectrum. At the degeneracy point, electron states on inequivalent ( $A/B$  or  $\tilde{A}/\tilde{B}$ ) sublattices in a single layer are decoupled, whereas interlayer coupling  $\gamma_{\tilde{A}B} \equiv \gamma_1$  forms dimers from pairs of  $\tilde{A}$ - $B$  orbitals in a bilayer [solid circles in Fig. 1], thus leading to the formation of high energy bands [13, 14].

The low energy states of electrons, as we show below, may be described by the effective Hamiltonian,

$$\begin{aligned} \hat{H}_2 &= -\frac{1}{2m} [\sigma_x (p_x^2 - p_y^2) + \sigma_y (p_x p_y + p_y p_x)] + \xi \hat{h}, \\ \hat{h} &= v_3 (\sigma_x p_x - \sigma_y p_y) + \end{aligned} \quad (1)$$

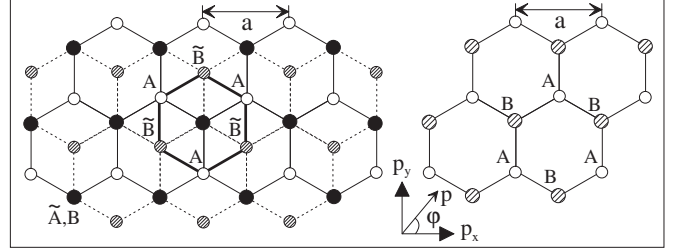


FIG. 1: Left: schematic of the bilayer lattice (bonds in the bottom layer  $A, B$  are indicated by solid lines and in the top layer  $\tilde{A}, \tilde{B}$  by dashed lines) containing four sites in the unit cell:  $A$  (white circles),  $\tilde{B}$  (hashed),  $\tilde{A}B$  dimer (solid). Right: the lattice of a monolayer.

$$+\frac{u}{2} \left( 1 - \frac{p^2}{2m^2 v^2} \right) \sigma_z + \frac{\hbar e B u}{4m^2 v^2} \sigma_0.$$

The Hamiltonian  $\hat{H}_2$  operates in the space of two component wave functions  $\Phi$  describing electronic amplitudes on  $A$  and  $\tilde{B}$  sites, for which we reserve  $2 \times 2$  Pauli matrices  $\sigma_i$  ( $\sigma_0 = 1$ ) [16]. In the valley  $K$ ,  $\xi = +1$ , we determine  $\Phi_{\xi=+1} = (\phi(A), \phi(\tilde{B}))$ , whereas in the valley  $\tilde{K}$ ,  $\xi = -1$  and the order of components is reversed,  $\Phi_{\xi=-1} = (\phi(\tilde{B}), \phi(A))$ .  $\hat{H}_2$  takes into account two possible ways of  $A \rightleftharpoons \tilde{B}$  hopping: via the dimer state (the main part) or due to a weak direct  $A\tilde{B}$  coupling,  $\gamma_{A\tilde{B}} \equiv \gamma_3 \ll \gamma_{\tilde{A}B}$  (the first line in  $\hat{h}$ ). They determine the mass  $m = \gamma_1/2v^2$  and velocity  $v_3 = (\sqrt{3}/2) a\gamma_{A\tilde{B}}/\hbar$ . Other weaker tunneling processes [7] are neglected. The second line of  $\hat{h}$  takes into account a possible asymmetry between top and bottom layers, opening a mini-gap  $\sim u$  in the bilayer spectrum. Finally,  $\mathbf{p} = -i\hbar\nabla - e\mathbf{A}$  takes into account a finite magnetic field  $\mathbf{B} = \text{rot}\mathbf{A}$ .

For comparison, the monolayer Hamiltonian [2],

$$\hat{H}_1 = \xi v (\sigma_x p_x + \sigma_y p_y),$$

is dominated by nearest neighbor intralayer hopping  $\gamma_{AB} = \gamma_{BA} \equiv \gamma_0 \gg \gamma_1$ , so that  $v = (\sqrt{3}/2) a\gamma_{AB}/\hbar$ . Comparison with equivalent parameters for bulk graphite [7] suggests that in  $\hat{H}_2$ , Eq. (1),  $v_3 \ll v$ . Thus, the first term in  $\hat{h}$ , which is similar to  $\hat{H}_1$ , is relevant only

for very small electron energies (i.e., in an electron gas with a very small density) whereas the energy spectrum within the interval  $\frac{1}{2}\gamma_1(v_3/v)^2 < \epsilon < \frac{1}{4}\gamma_1$  is dominated by the main term in  $\hat{H}_2$  producing a quadratic dispersion  $|\epsilon| = p^2/(2m)$ , which contrasts with linear dispersion  $|\epsilon| = vp$  in a monolayer. Below, we extend this comparison onto the spectrum of Landau levels and the resulting sequencing of quantum Hall effect plateaus in  $\sigma_{xy}$ .

A microscopic analysis leading to the bilayer Hamiltonian  $\hat{H}_2$  is based on the tight-binding model of graphite using the Slonczewski-Weiss-McClure parameterization [7] of relevant couplings. We quote experimental values of relevant hopping parameters,  $v = 8.0 \times 10^5 m/s$  from Ref. 10,  $\gamma_1 = 0.39 eV$  and  $\gamma_3 = 0.315 eV$  from Ref. 7, and we neglect the weakest coupling  $\gamma_{A\bar{A}} = \gamma_{B\bar{B}} \equiv \gamma_4 = 0.044 eV$ . For convenience, we represent the Hamiltonian near the centers of the valleys in a basis with components corresponding to atomic sites  $A, \bar{B}, \bar{A}, B$  in the valley  $K$  [15] and to  $\bar{B}, A, B, \bar{A}$  in the valley  $\bar{K}$ :

$$\mathcal{H} = \xi \begin{pmatrix} \frac{1}{2}u & v_3\pi & 0 & v\pi^\dagger \\ v_3\pi^\dagger & -\frac{1}{2}u & v\pi & 0 \\ 0 & v\pi^\dagger & -\frac{1}{2}u & \xi\gamma_1 \\ v\pi & 0 & \xi\gamma_1 & \frac{1}{2}u \end{pmatrix}; \quad \begin{cases} \pi = p_x + ip_y, \\ \mathbf{p} = -i\hbar\nabla - e\mathbf{A}, \\ [\pi, \pi^\dagger] = 2\hbar eB. \end{cases}$$

Here  $u$  distinguishes between on-site energies in the two layers,  $\epsilon_{A,B} = \frac{1}{2}u$  and  $\epsilon_{\bar{A},\bar{B}} = -\frac{1}{2}u$  (e.g., a substrate effect).

The Hamiltonian  $\mathcal{H}$  determines the following spectrum of electrons in a bilayer at zero magnetic field. There are four valley-degenerate bands,  $\epsilon_\alpha^\pm(\mathbf{p})$ ,  $\alpha = 1, 2$ , with

$$\epsilon_\alpha^\pm = \frac{\gamma_1^2}{2} + \frac{u^2}{4} + \left(v^2 + \frac{v_3^2}{2}\right)p^2 + (-1)^\alpha \left[ \frac{(\gamma_1^2 - v_3^2 p^2)^2}{4} + v^2 p^2 [\gamma_1^2 + u^2 + v_3^2 p^2] + 2\xi\gamma_1 v_3 v^2 p^3 \cos 3\varphi \right]^{1/2},$$

where  $\tan \varphi = p_y/p_x$ . Here,  $\epsilon_2$  describes a pair of higher energy bands formed by  $\bar{A}\bar{B}$  dimers with  $|\epsilon| \gtrsim \gamma_1$ , and  $\epsilon_1$  describes low energy states whose properties are the focus of this paper.

The dispersion in the intermediate energy range,  $\frac{1}{2}\gamma_1(v_3/v)^2, u < |\epsilon| < \gamma_1$ , can be approximated with

$$\epsilon_1^\pm \approx \pm \frac{1}{2}\gamma_1 \left[ \sqrt{1 + 4v^2 p^2 / \gamma_1^2} - 1 \right]. \quad (2)$$

This corresponds to the effective mass for electrons near the Fermi energy in a 2D gas with density  $N$ ,  $m_c = p/(\partial\epsilon/\partial p) = \gamma_1/(2v^2) \sqrt{1 + 4\pi\hbar^2 v^2 N/\gamma_1^2}$ . The relation in Eq. (2) interpolates between a linear spectrum  $\epsilon \approx vp$  at high momenta and a quadratic spectrum  $\epsilon \approx p^2/2m$ , where  $m = \gamma_1/2v^2$ . Such a crossover happens at  $p \approx \gamma_1/(2v)$ , which corresponds to the carrier density  $N^* \approx \gamma_1^2/(4\pi\hbar^2 v^2)$ . The experimental graphite values [7, 10] give  $N^* \approx 4.36 \times 10^{12} cm^{-2}$ , whereas the dimer band  $\epsilon_2$  becomes occupied only if the carrier density exceeds  $N^{(2)} \approx 2\gamma_1^2/(\pi\hbar^2 v^2) \approx 8N^* \approx 3.49 \times 10^{13} cm^{-2}$ . The

estimated effective mass  $m$  is “light”:  $m \approx 0.054m_e$  using the above quoted values [7, 10] or  $m \approx 0.014m_e$  using a theoretical bilayer value  $\gamma_1 = 0.1eV$  [13].

The  $4 \times 4$  Hamiltonian  $\mathcal{H}$  contains information about the higher energy band  $\epsilon_2$ , and, therefore, is not convenient for the analysis of transport properties of a bilayer which are formed by carriers in the low energy band  $\epsilon_1$ . We separate  $\mathcal{H}$  into  $2 \times 2$  blocks, where the upper left diagonal block is  $H_{11} \equiv \xi(\frac{1}{2}u\sigma_z + v_3[\sigma_x p_x - \sigma_y p_y])$ , the lower right diagonal block is  $H_{22} = -\frac{1}{2}\xi u\sigma_z + \gamma_1\sigma_x$ , and the off-diagonal blocks are  $H_{21} = H_{12} = v\xi(\sigma_x p_x + \sigma_y p_y)$ . Then, we take the  $4 \times 4$  Green function determined by  $\mathcal{H}$ , evaluate the block  $G_{11}$  related to the lower-band states, and use it to identify the effective low-energy bilayer Hamiltonian  $\hat{H}_2$ . Following this route, we write

$$G = \begin{pmatrix} G_{11} & G_{12} \\ G_{21} & G_{22} \end{pmatrix} = \begin{pmatrix} G_{11}^{(0)-1} & H_{12} \\ H_{21} & G_{22}^{(0)-1} \end{pmatrix}^{-1} \equiv (\mathcal{H} - \epsilon)^{-1},$$

where  $G_{\alpha\alpha}^{(0)} = (H_{\alpha\alpha} - \epsilon)^{-1}$ . Then, we find that  $G_{11} = \left(1 - G_{11}^{(0)} H_{12} G_{22}^{(0)} H_{21}\right)^{-1} G_{11}^{(0)}$ , so that  $G_{11}^{-1} + \epsilon = H_{11} - H_{12} G_{22}^{(0)} H_{21}$ . Since  $|\epsilon| \ll \gamma_1$ , we expand  $G_{22}^{(0)} = (H_{22} - \epsilon)^{-1}$  in  $\gamma_1^{-1}$  [17], keeping only terms up to quadratic in  $\mathbf{p}$  (and therefore in  $\pi^\dagger, \pi$ ), and arrive at

$$\hat{H}_2 = -\frac{v^2}{\gamma_1} \begin{pmatrix} 0 & (\pi^\dagger)^2 \\ \pi^2 & 0 \end{pmatrix} + \xi v_3 \begin{pmatrix} 0 & \pi \\ \pi^\dagger & 0 \end{pmatrix} + \xi u \left[ \frac{1}{2} \begin{pmatrix} 1 & 0 \\ 0 & -1 \end{pmatrix} - \frac{v^2}{\gamma_1^2} \begin{pmatrix} \pi^\dagger \pi & 0 \\ 0 & -\pi \pi^\dagger \end{pmatrix} \right]. \quad (3)$$

The latter expression may be equivalently represented in the form Eq. (1) using  $m = \gamma_1/(2v^2)$ . The two component eigenstates  $\Phi$  of  $\hat{H}_2$  correspond to atomic sites  $(A, \bar{B})$  in the valley  $K$  and to  $(\bar{B}, A)$  in the valley  $\bar{K}$  [15], and the operator  $\pi = p_x + ip_y$  incorporates the vector potential due to magnetic field.

For low quasiparticle energies,  $|\epsilon| \ll \gamma_1$ , the spectrum determined by  $\hat{H}_2$  in Eqs. (1,3) agrees with  $\epsilon_1(p)$  found using the  $4 \times 4$  Hamiltonian  $\mathcal{H}$ . Similarly to bulk graphite [7, 18], the effect of a small  $v_3$  term consists of trigonal warping, which deforms the isoenergetic lines along the directions  $\varphi = \varphi_0$ , as shown in Fig. 2. For the valley  $K$ ,  $\varphi_0 = 0, \frac{2}{3}\pi$  and  $\frac{4}{3}\pi$ , whereas for  $\bar{K}$ ,  $\varphi_0 = \pi, \frac{1}{3}\pi$  and  $\frac{5}{3}\pi$ . At the lowest energies  $|\epsilon| < \frac{1}{2}\gamma_1(v_3/v)^2$ , trigonal warping breaks the isoenergetic line into four pockets, which can be referred to as one “central” and three “leg” parts [18]. The central part and leg parts have minimum  $|\epsilon| = \frac{1}{2}u$  at  $p = 0$  and at  $|p| = \gamma_1 v_3 / v^2$ , angle  $\varphi_0$ , respectively. For  $v_3 \sim 0.1v$ , we find (using the data in Ref. 7) that the separation of a 2D Fermi line into four pockets would take place for very small carrier densities  $N < N_c = 2(v_3/v)^2 N^* \sim 1 \times 10^{11} cm^{-2}$ . For such small densities, the central part of the Fermi surface is approximately circular with area  $\mathcal{A}_{\text{cent}} \approx \pi\epsilon^2/(\hbar v_3)^2$ , and each leg part is elliptical with area  $\mathcal{A}_{\text{leg}} \approx \frac{1}{3}\mathcal{A}_{\text{cent}}$  [19]. This determines the following sequencing of the first few LL’s

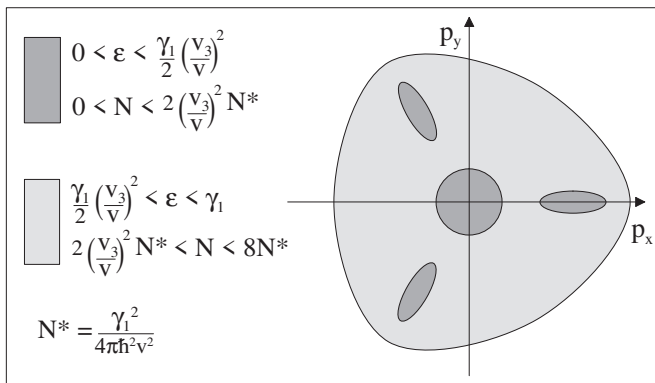


FIG. 2: Schematic of the Fermi line in the valley  $K$ ,  $\xi = 1$ , for high (light shading) and low density (dark shading).

in the low magnetic field spectrum of a low-density bilayer ( $B \lesssim B_c \approx hN_c/4e \sim 1T$  and  $N < N_c$ ). Every third Landau level from the central part has the same energy as levels from each of the leg pockets, resulting in groups of four degenerate states. These groups of four would be separated by pairs of non-degenerate levels arising solely from the central pocket.

In structures with densities  $N \gg N_c$  or for strong magnetic fields  $B \gg B_c$ , the above described LL spectrum evolves into an almost equidistant staircase of levels. We derive such a spectrum numerically from Eq. (3) using the Landau gauge  $\mathbf{A} = (0, Bx)$ , in which the pair of operators  $\pi^\dagger$  and  $\pi$  are nothing but the pair of raising and lowering operators in the basis of standard LL functions  $e^{iky} \phi_n(x)$  where  $\phi_n$  are magnetic oscillator eigenstates [20]. They obey  $\pi^\dagger \phi_n = i(\hbar/\lambda_B) \sqrt{2(n+1)} \phi_{n+1}$ ,  $\pi \phi_n = -i(\hbar/\lambda_B) \sqrt{2n} \phi_{n-1}$ , and  $\pi \phi_0 = 0$ , where  $\lambda_B = \sqrt{\hbar/(eB)}$ . In this we followed an approach applied earlier to bulk graphite [18] and used the bulk parameters for intralayer  $v$  and interlayer  $\gamma_1$ , varying the value of the least known parameter  $v_3$ . The spectrum for the valley  $K$  ( $\xi = 1$ ) is shown in Fig. 3 as a function of the ratio  $v_3/v$  for two different fields. Fig. 3(a) shows the evolution of the twenty lowest levels for  $B = 0.1T$  as a function of  $v_3$ , illustrating the above-mentioned crossover from an equidistant ladder at  $v_3 = 0$  to groups of pocket-related levels.

The result obtained for a larger field, Fig. 3(b), shows that for  $B = 1T$  the LL spectrum is almost independent of  $v_3$  over a broad range of its values. Therefore, even in the absence of a definite value of this parameter, we are confident that the LL spectrum in bilayers studied over a few Tesla range of magnetic field (as in recent experiments on ultra-thin films [8, 10]) can be adequately described by neglecting  $v_3$ , thus using an approximate Hamiltonian given by the first term in  $\hat{H}_2$ , Eqs. (1,3).

The resulting spectrum contains a ladder of almost equidistant energy levels,

$$\epsilon_n^\pm = \pm \hbar\omega_c \sqrt{n(n-1)} - \frac{1}{2} \xi \delta, \quad \text{for } n \geq 2, \quad (4)$$

which are weakly split in valleys  $K$  ( $\xi = +1$ ) and  $\tilde{K}$

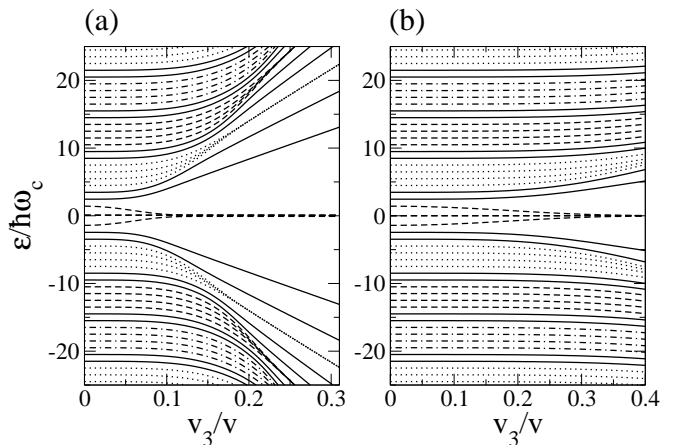


FIG. 3: Numerically calculated Landau levels for various values of  $v_3$  for valley  $K$ ,  $\xi = 1$ . (a) for  $B = 0.1T$  ( $\hbar\omega_c = 0.216meV$  assuming  $\gamma_1 = 0.39eV$ ,  $u/\gamma_1 = 0.0001$  and  $v = 8.0 \times 10^5 m/s$ ), (b) for  $B = 1T$  ( $\hbar\omega_c = 2.16meV$ ). Broken lines show groups of four consecutive levels that become degenerate at large  $v_3$ , with each group separated from the next by two solid lines representing levels that are not degenerate.

( $\xi = -1$ ),  $\delta = u\hbar\omega_c/\gamma_1$ . Here  $\omega_c = eB/m$ , and  $\epsilon_n^+$  and  $\epsilon_n^-$  are assigned to electron and hole states, respectively. The eigenstates corresponding to these levels are

$$\Phi_{n\xi} \equiv C_{n\xi} (\phi_n, D_{n\xi} \phi_{n-2}), \quad \text{for } n \geq 2, \quad (5)$$

where  $D_{n\xi} = [\epsilon - \xi u/2 + \xi n \delta]/(\hbar\omega_c \sqrt{n(n-1)})$  and  $C_{n\xi} = 1/\sqrt{1 + |D_{n\xi}|^2}$ . In the limit of valley ( $u = 0$ ) and spin degeneracies, we shall refer to these states as 4-fold degenerate LL's.

The LL spectrum in each valley also contains two nearly degenerate levels which can be identified using the fact that  $\pi^2 \phi_1 = \pi^2 \phi_0 = 0$ ,

$$\begin{cases} \epsilon_0 = \frac{1}{2} \xi u; & \Phi_{0\xi} \equiv (\phi_0, 0); \\ \epsilon_1 = \frac{1}{2} \xi u - \xi \delta; & \Phi_{1\xi} \equiv (\phi_1, 0). \end{cases} \quad (6)$$

According to different definitions of two-component  $\Phi$  in two valleys,  $n = 0, 1$  LL states in the valley  $K$  are formed by orbitals predominantly on the  $A$  sites from the bottom layer, whereas the corresponding states in the valley  $\tilde{K}$  are located on  $\tilde{B}$  sites from the top layer, which is reflected by the splitting  $u$  between the lowest LL in the two valleys. In a gapless bilayer ( $u = 0$ ) levels  $\epsilon_0$  and  $\epsilon_1$  are degenerate and have the same energy in valleys  $K$  and  $\tilde{K}$ , thus forming an 8-fold degenerate LL at  $\epsilon = 0$  (here we also take into account electron spin).

Having in mind the range of field  $B \gtrsim 1T$ , we aim to relate the LL spectrum in Eqs. (4,6) to the density dependence of QHE  $\sigma_{xy}$  in a bilayer system. We assume that finite temperature, LL broadening due to disorder and sample inhomogeneity hinder small valley and spin splittings as well as the splitting between  $n = 0, 1$  electron/hole LL's in Eqs. (6), and the percolating states

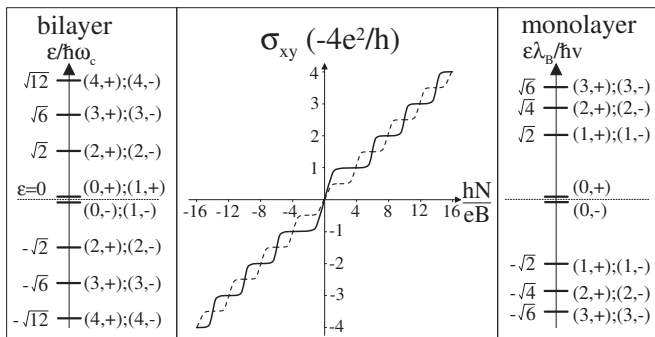


FIG. 4: Landau levels for a bilayer (left) and monolayer (right). Brackets  $(n, \xi)$  indicate LL number  $n$  and valley index  $\xi = \pm 1$ . In the center the predicted Hall conductivity  $\sigma_{xy}$  (center) as a function of carrier density for bilayer (solid line) is compared to that of a monolayer (dashed line).

from these levels would overlap. Thus, the Hall conductivity dependence on carrier density,  $\sigma_{xy}(N)$ , would reflect [20] the presence of groups of 4 spin- and valley-degenerate LL's with  $n \geq 2$ , and the group of 8 states at  $|\epsilon| = 0$  (4 for electrons and 4 for holes), as shown in Fig. 4. A solid line sketches the form of  $\sigma_{xy}(N)$  in the QHE regime in a bilayer which exhibits plateaus at integer values of  $4e^2/h$  and has a “double”  $8e^2/h$  step

between the hole and electron gases across  $N = 0$ .

This behavior contrasts with that of a monolayer which has a spectrum containing 4-fold (spin and valley) degenerate LL [1],  $\epsilon_0 = 0$ ,  $\epsilon_{n \geq 1}^{\pm} = \pm \sqrt{2n} \hbar v / \lambda_B$ , shown on the r.h.s of Fig. 4. Such a spectrum corresponds to Hall conductivity  $\sigma_{xy}(N)$  which is plotted as a dotted line and exhibits plateaus at half-integer multiples of  $4e^2/h$ , as discussed in earlier publications [6].

The above-described peculiarities of the spectrum of bilayer graphite show that monolayer and bilayer systems can be distinguished on the basis of Hall conductivity measurements. Indeed, the recent Hall effect study of ultra-thin films by Novoselov *et al.* [10] featured two types of  $\sigma_{xy}(N)$  dependence shown in Fig. 4, which we interpret as an indication that the fabrication process used in it generated both single and bilayer samples. It is also worth mentioning that the 8-fold degeneracy of the group of  $\epsilon = 0$  LL's, Eqs. (6), is quite unusual in 2D systems. It suggests that e-e interaction in a bilayer may give rise to a variety of strongly correlated QHE states. For structures studied in Ref. 10, with electron/hole densities  $N \sim 10^{12} \text{cm}^{-2}$ , such a regime may be realized in fields  $B \sim 10T$ .

The authors thank A. Geim, K. Novoselov, and I. Aleiner for useful discussions, and EPSRC for support.

- 
- [1] J. W. McClure, Phys. Rev. **104**, 666 (1956).  
[2] D. P. DiVincenzo and E. J. Mele, Phys. Rev. B **29**, 1685 (1984); C. L. Kane and E. J. Mele, Phys. Rev. Lett. **78**, 1932 (1997).  
[3] C. de C. Chamon, C. Mudry, and X.-G. Wen, Phys. Rev. Lett. **77**, 4194 (1996); D. H. Kim, P. A. Lee, X. G. Wen, Phys. Rev. Lett. **79**, 2109 (1997); Y. Hatsugai and P. A. Lee, Phys. Rev. B **48**, 4204 (1993).  
[4] D. V. Khveshchenko, Phys. Rev. Lett. **87**, 206401 (2001).  
[5] J. González, F. Guinea, and M. A. H. Vozmediano, Phys. Rev. B **63**, 134421 (2001); T. Stauber, F. Guinea, and M. A. H. Vozmediano, Phys. Rev. B **71**, 041406 (2005).  
[6] Y. Zheng and T. Ando, Phys. Rev. B **65**, 245420 (2002); V. P. Gusynin and S. G. Sharapov, Phys. Rev. Lett. **95**, 146801 (2005).  
[7] M. S. Dresselhaus and G. Dresselhaus, Adv. Phys. **51**, 1 (2002); R. C. Tatar and S. Rabi, Phys. Rev. B **25**, 4126 (1982); J.-C. Charlier, X. Gonze, and J.-P. Michenaud, Phys. Rev. B **43**, 4579 (1991). The Slonczewski-Weiss-McClure band model of bulk graphite has seven parameters, but couplings  $\gamma_2$  and  $\gamma_5$  do not appear in a bilayer.  
[8] K. S. Novoselov *et al.*, Science **306**, 666 (2004).  
[9] K. S. Novoselov *et al.*, PNAS **102**, 10451 (2005); J. S. Bunch *et al.*, Nano. Lett. **5**, 287 (2005); Y. Zhang *et al.*, Phys. Rev. Lett. **94**, 176803 (2005); C. Berger *et al.*, J. Phys. Chem. B **108**, 19912 (2004).  
[10] K. S. Novoselov *et al.*, cond-mat/0509330.  
[11] Y. Zhang *et al.*, cond-mat/0509355.  
[12] S. Horiuchi *et al.* Appl. Phys. Lett. **84**, 2403 (2004).  
[13] S. B. Trickey *et al.*, Phys. Rev. B **45**, 4460 (1992).  
[14] K. Yoshizawa, T. Kato, and T. Yamabe, J. Chem. Phys. **105**, 2099 (1996); T. Yumura and K. Yoshizawa, Chem. Phys. **279**, 111 (2002).  
[15]  $K$  and  $\tilde{K}$  wave vectors are  $\mathbf{K}_{\xi} = \xi(\frac{4}{3}\pi a^{-1}, 0)$  where  $\xi = \pm 1$  and  $a$  is the hexagonal lattice constant.  
[16] In application to  $\hat{H}_2$ , time reversal is described by  $(\Pi_1 \otimes \sigma_x) \hat{H}^* (\mathbf{p}, B, u) (\Pi_1 \otimes \sigma_x) = \hat{H} (-\mathbf{p}, -B, u)$ , spatial inversion by  $(\Pi_1 \otimes \sigma_0) \hat{H} (\mathbf{p}, B, u) (\Pi_1 \otimes \sigma_0) = \hat{H} (-\mathbf{p}, B, -u)$ , where  $\Pi_1$  swaps  $\xi = +1$  and  $\xi = -1$  in valley space.  
[17] First we use  $G_{22}^{(0)} = \gamma_1^{-1} \sigma_x + \epsilon \gamma_1^{-2} \sigma_0 - \frac{1}{2} \xi u \gamma_1^{-2} \sigma_z + O(\gamma_1^{-3})$ . Then, we consider the energy eigenvalue equation  $(G_{11}^{-1} + \epsilon) \psi = \epsilon \psi$  and collect the terms containing  $\epsilon$  on one side,  $(1 + \gamma_1^{-2} H_{12}^2) \epsilon \psi = (H_{11} - \gamma_1^{-1} H_{12} \sigma_x H_{21} + \frac{1}{2} \xi u \gamma_1^{-2} H_{12} \sigma_z H_{21}) \psi$ . Multiplying both sides as  $(1 + \gamma_1^{-2} H_{12}^2)^{-1/2} \{ \dots \} (1 + \gamma_1^{-2} H_{12}^2)^{-1/2}$ , and keeping terms up to  $\gamma_1^{-2}$ , we find  $H_2 = H_{11} - \gamma_1^{-1} H_{12} \sigma_x H_{21} - \frac{1}{2} \gamma_1^{-2} \{ H_{12}^2, H_{11} \} + \frac{1}{2} \xi u \gamma_1^{-2} H_{12} \sigma_z H_{21}$  where  $\{ H_{12}^2, H_{11} \} = H_{12}^2 H_{11} + H_{11} H_{12}^2$ .  
[18] G. Dresselhaus, Phys. Rev. B **10**, 3602 (1974); K. Nakao, J. Phys. Soc. Japan, **40**, 761 (1976); M. Inoue, J. Phys. Soc. Japan, **17**, 808 (1962); O. P. Gupta and P. R. Wallace, Phys. Stat. Sol. B **54**, 53 (1972).  
[19] For  $\epsilon^2 \ll \frac{1}{4} \gamma_1^2 (v_3/v)^4 + \frac{1}{4} u^2$ , behavior on the leg pocket may be described analytically by shifting the momentum in the effective Hamiltonian Eq. (3) by  $\pi \rightarrow \pi + (\gamma_1 v_3/v^2) \exp(i\varphi_0)$ , and then taking  $m^{-1} \rightarrow 0$ . This yields an elliptical Fermi surface  $\epsilon^2 = \frac{1}{4} u^2 (1 - 2v_3^2/v^2)^2 + v_3^2 p^2 (5 - 4 \cos[2(\varphi - \varphi_0)])$ , and for finite magnetic field gives levels with  $\epsilon_0 = \frac{1}{2} \xi u (1 - 2v_3^2/v^2)$  and  $\epsilon_{n \geq 1} = \pm [6n(\hbar v_3/\lambda_B)^2 + \frac{1}{4} u^2 (1 - 2v_3^2/v^2)^2]^{1/2}$ .

- [20] “*The Quantum Hall Effect*”, edited by R. E. Prange and S. M. Girvin (Springer-Verlag, New York, 1986).